New inhibitors of *Mycobacterium tuberculosis* identified using systems chemical biology

Eachan O. Johnson[1,2,3], Emily LaVerriere[1], Mary Stanley[1], Emma Office[1], Elisabeth Meyer[1], Tomohiko Kawate[1,2,3], James Gomez[1], Rebecca E. Audette[4], Nirmalya Bandyopadhyay[1], Natalia Betancourt[5], Kayla Delano[1], Israel Da Silva[5], Joshua Davis[1], Christina Gallo[1], Michelle Gardner[6], Aaron Golas[1], Kristine M. Guinn[6], Rebecca Korn[1], Jennifer A. McConnell[5], Caitlin E. Moss[6], Kenan C. Murphy[4], Ray Nietupski[1], Kadamba G. Papavinasasundaram[4], Jessica T. Pinkham[6], Paula A. Pino[5], Megan K. Proulx[4], Nadine Ruecker[5], Naomi Song[5], Matthew Thompson[1], Carolina Trujillo[5], Shoko Wakabayashi[6], Joshua B. Wallach[5], Christopher Watson[1], Thomas R. Ioerger[7], Eric S. Lander[1], Brian K. Hubbard[1], Michael H. Serrano-Wu[1], Sabine Ehrt[5], Michael Fitzgerald[1], Eric J. Rubin[6], Christopher M. Sassetti[4], Dirk Schnappinger[5], Deborah T. Hung[1,2,3*]

With the rise in antibiotic resistance, new drugs are desperately needed against *Mycobacterium tuberculosis* (Mtb). Combining chemistry and genetics, we developed a new strategy for rapidly identifying many new small molecule candidates against Mtb and shedding light on their mechanisms of action (MOA), by performing large-scale chemical screening on pooled genetic libraries containing >100 barcoded strains hypomorphic for individual essential genes. We created barcoded hypomorphic strains for 474 of the $\sim\sim 625$ essential genes in Mtb and developed a multiplexed, whole-cell assay to measure strain abundance. Applying the approach with an activity-enriched, 3226 compound library and an unbiased 47,353 compound library, we characterized >8.5 million chemical-genetic interactions. Using machine learning, we identified >40 novel compounds against known MOAs, including new inhibitors of DNA gyrase, mycolic acid biosynthesis, and folate biosynthesis. By identifying highly specific chemical-genetic interactions, we identified new inhibitors of RNA polymerase and of a novel target, EfpA. Finally, we showed an inhibitor discovered by screening the hypomorphic strains could be optimized by medicinal chemistry to be active against wild-type Mtb. The results demonstrate that a systems chemical biology approach can empower discovery, prioritization, and development of compounds towards novel TB therapeutics.

Tuberculosis (TB) imposes an enormous global burden, causing more than 1.6 million deaths annually (1). Although curative chemotherapies were developed in the mid-20th century (2), TB became the deadliest infectious disease worldwide in 2016, fueled partly by the HIV epidemic. At the same time, TB has become harder to treat due to increasing prevalence of multi-drug resistant (MDR) TB (defined as resistance to two front-line drugs, rifampin (RIF) and isoniazid (INH)) and the emergence of extensively (XDR) and totally drug resistant (TDR) TB (3). Controlling TB requires concerted public health and social efforts, coupled with new diagnostics and therapeutics. Despite the recent approval of two new drugs (bedaquiline and delamanid), TB drug development remains slow, hampered by a paucity of validated targets in the causative bacterium, *Mycobacterium tuberculosis* (Mtb), and a limited number of active compounds with favorable chemical characteristics that could serve as lead candidates. New targets and drug leads are desperately needed.

A major challenge has been the difficulty of identifying the molecular targets of compounds found to inhibit TB in whole-cell screens to enable chemical optimization. In the few cases where mechanism-of-action (MOA) has been illuminated, the targets often belong to the same small set of membrane proteins (such as MmpL3 and DprE1). For the vast majority of the ~625 essential genes in Mtb, no chemical inhibitors are known (4-6).

To accelerate drug discovery, we took a systems chemical biology approach involving multiplex chemical screening of genetic libraries of hundreds of mutant strains. We genetically engineered 474 hypomorphic Mtb strains, each depleted for a different essential gene product and each carrying a distinct genetic barcode. We then screened compounds against a pool of 100 strains (99 hypomorphs and wildtype), determined the sensitivity of each strain to each compound from the abundance of the barcodes, and made inferences about the MOA of compounds from the sensitivity pattern across depletion strains. The approach is based on the concept that strains depleted for a protein tend to be hypersensitive to drugs targeting the protein (7)–an idea first championed in yeast and applied in the discovery of platensimycin in Staphylococcus aureus (8) and recent screening of individual depleted strains of Mtb (9, 10).

We validated the approach on a collection of 3226 small molecules enriched for anti-Mtb activity. We successfully predicted MOA of novel compounds against known targets based on similar sensitivity patterns to compounds with known MOA, resulting in the discovery of new inhibitors of DNA gyrase, cell wall biosynthesis, and folate biosynthesis. We also

[1]Broad Institute of MIT and Harvard, 415 Main Street, Cambridge, MA 02139, USA.
[2]Department of Molecular Biology and Center for Computational and Integrative Biology, Massachusetts General Hospital, 185 Cambridge Street, Simches 7, Boston, MA 02114, USA.
[3]Department of Genetics, Harvard Medical School, Boston, MA 02115, USA.
[4]Department of Immunology and Infectious Diseases, Harvard TH Chan School of Public Health, Boston, MA, 02115, USA.
[5]Department of Microbiology and Immunology, Weill Cornell Medical College, New York, NY, 10021, USA.
[6]Department of Microbiology and Physiological Systems, University of Massachusetts Medical School, Worcester, MA, 01655, USA.
*Correspondence to: hung@broadinstitute.org

identified compounds against targets based on their ability to inhibit specific knockdown strains, leading to the identification of novel inhibitors of RNA polymerase (RNAP) and the essential efflux pump EfpA, a new and uncharacterized target. In the latter case, we were able to optimize the initial compound so that it inhibited not only the EfpA-depletion strain, but also wild-type Mtb.

Finally, we demonstrate the expansion of this strategy to screen a library of 47,353 compounds against 151 depletion strains. This screen showed ∼10-fold greater sensitivity over screening wild-type Mtb alone, and led to the identification of ∼1500 new small molecules, each associated with activity against specific subsets of Mtb depletion strains. By optimizing the EfpA inhibitor so that it inhibited not only the EfpA-depletion strain, but also wild-type Mtb, we showed that compounds discovered through mutant hypersensitivity could be developed to have pharmacologically-relevant potency against Mtb.

The new screening approach and new chemical hits should help accelerate TB drug development.

Development of a multiplexed chemical genetic screening platform in Mtb

We constructed knockdown strains targeting 474 of the ∼625 essential genes defined in Mtb–including genes that are absolutely essential, are severely growth defective, or have essential domains (11). Hypomorphic strains of Mtb H37Rv were created by placing an essential gene under conditional proteolytic control using a tetracycline-repressible SspB:DAS degradation system (12, 13), or conditional transcriptional control through promoter replacement for some membrane proteins (Table S1). For proteolytic control, proteins were fused to a carboxy-terminal DAS-tag, which targets the protein for degradation *via* SspB-dependent shuttling. Up to five different engineered strains for each gene were created, with varying degrees of knockdown based on the strength of the promoter driving sspB expression and thus the degree of degradation (Fig. S1A). In total, we created 2014 strains.

Each strain was also engineered to carry a 20-nucleotide genetic barcode flanked by common primer-binding sites (Fig. S1B) for targeted gene identification by multiplexed polymerase chain reaction (PCR) and next generation sequencing (NGS). Sequencing reads of the barcode were intended to serve as a proxy for strain census in a pooled context.

We developed an assay to measure the abundance of each strain in a pool, by PCR amplifying and sequencing the barcodes (Fig. 1A) (14-17). We confirmed that barcode counts were an accurate proxy for strain abundance, by mixing strains at known abundances spanning three orders of magnitude ($r = 0.93$ for log-transformed barcode count replicates; $r = 0.95$ for known cell abundance and barcode counts) (Fig. 1B).

We performed high-throughput chemical screen of a pool containing 100 strains (99 hypomorphs and wild-type H37Rv). Using the barcode quantification, we determined the growth rate of each pooled strain in 384-microwell broth culture over two weeks. From the multiple strains constructed for each gene, we selected the strain with the strongest degradation with proliferation most similar to the wild-type strain. This growth-matched pool was used for all subsequent multiplexed experiments.

We optimized screening assay parameters in 384-well format, including compound exposure time (14 days), genomic DNA extraction (10% dimethylsulfoxide (DMSO) and 95°C for 15 min), and PCR conditions (20 cycles, annealing at 65°C) that maximized the robust Z'-score of log-transformed counts for a RIF dilution series (Table S2) and minimized random noise as determined by strain-wise coefficient of variance (CV) (Table S3).

An appropriate sequencing depth (500 reads per strain per well) was determined by performing repeated simulations of a 10,000-well high-throughput screening dataset with active compounds present at 1%, balancing cost, accuracy, sensitivity, and inference of fitness (*via* a generalized linear model). We developed our analysis protocol into a pipeline, ConCensusGLM, that calculates, for each unique strain, compound, and concentration combination, a $\log_2$(fold change) (LFC, interpreted as chemical-genetic interaction score) of counts relative to the DMSO control screening wells, and a p-value (Wald test).

Screening a library of known Mtb-active compounds

We assembled a library of 3226 small-molecules enriched for compounds with activity against wild-type Mtb. The library was drawn from a pool of 1128 compounds we had identified in internal screening efforts as having activity against wild-type Mtb H37Rv (18-20), 5611 compounds reported by Southern Research Institute (21-23), and 177 compounds reported by GlaxoSmithKline (24). After removing duplicates, we assembled a library of 2000 available compounds. We supplemented this collection with 1226 compounds from Selleck's Pharmacologically Active Compound Library, to include known antibiotics to serve as positive controls and as ground truth data for machine learning. To confirm the reported Mtb activity, we screened the library against GFP-expressing wild-type Mtb H37Rv (22) and found that 1312 (45%) had an $MIC_{90} < 64$ μM.

We then screened the compound library against our pool of 100 Mtb strains in duplicate (log-transformed Pearson's $r = 0.93$). Because fitness differences between a given hypomorph and wild-type Mtb can depend on compound concentration, we screened at four library concentrations: 1.1, 3.3, 10, and 30 μM (chosen based on measured MIC_{90} values for the entire library).

The screen readily identified chemical-genetic interactions between compounds and hypomorphic strains for their known targets. For example, the fluoroquinolones selectively inhibited the DNA gyrase α-subunit (GyrA) hypomorph, a known interaction that occurs at extreme depletion of GyrA (Fig. 1C). RIF inhibited the hypomorph for the β-subunit of its known target, RNAP (RpoB) (Fig. 1C). The tryptophan syn-

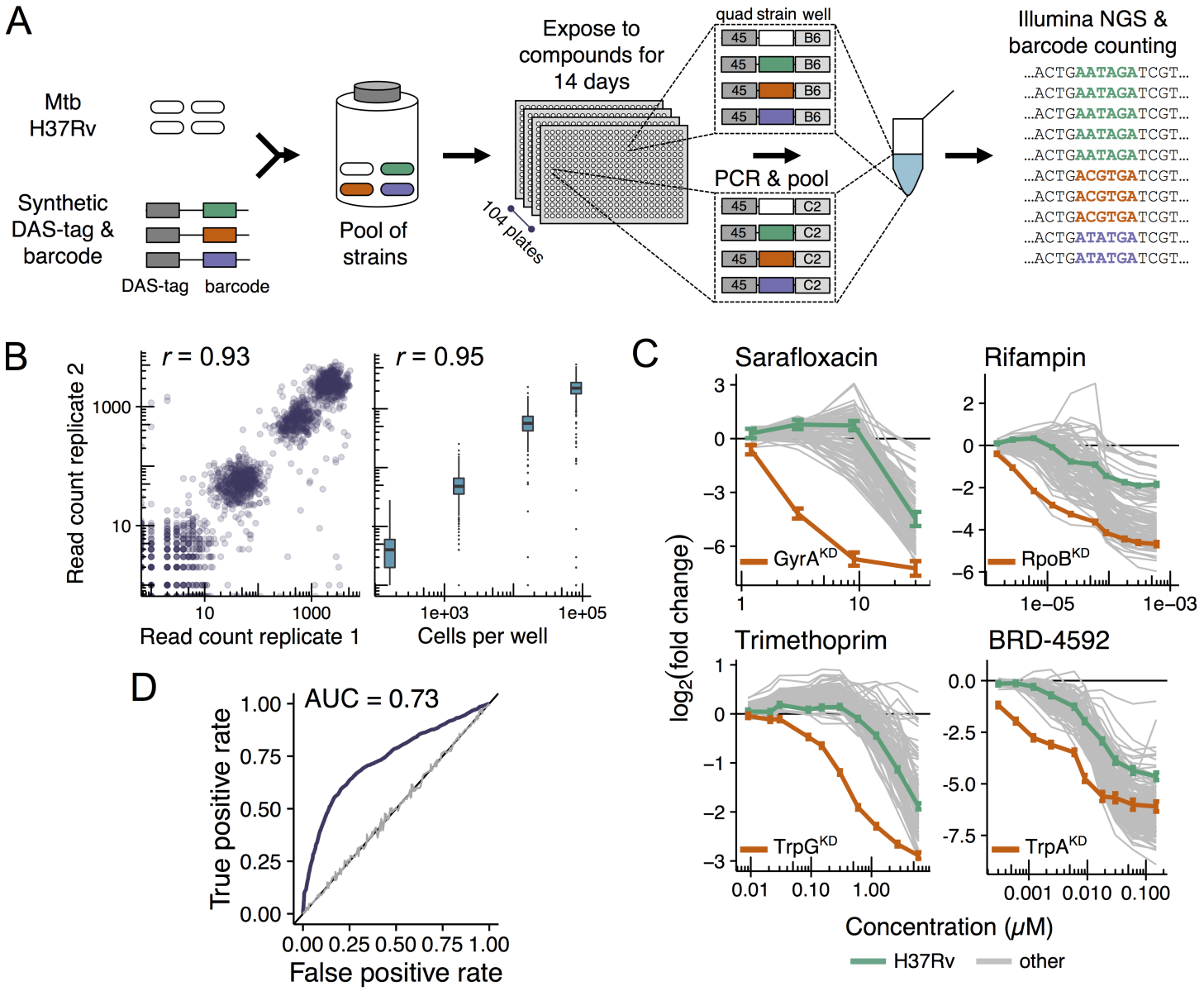

Figure 1: Multiplexed screening of genetically barcoded hypomorph strains of Mtb is reliable, reproducible, and provides MOA insight. (**A**) Strains were constructed by introducing a DAS-tag into the locus of the gene of interest, with concomitant genetic barcoding and introduction of regulated SspB expression to control the level of protein depletion. Hypomorph strains were pooled and distributed into 384-well plates containing the compound library and incubated for 14 days. After heat inactivation, the chromosomal barcodes were PCR amplified by an array of primers containing 5′-overhangs incorporating screen location barcodes. PCR products were pooled and subjected to Illumina NGS. (**B**) Known mixtures of barcoded wild type H37Rv strains were subjected to census estimation by barcode counting. The method is reproducible with a log-transformed Pearson's $r = 0.93$ (left panel) and allows accurate estimation of strain relative abundance with Pearson's $r = 0.95$ (right panel). (**C**) Chemical genetic interaction profiles from screen data showed expected hypersensitivity for compounds of known MOA. Profiles show the LFC (relative to DMSO negative controls) of each strain at each concentration tested, with wild-type Mtb H37Rv highlighted in green and a mutant of interest highlighted in orange. Error bars of highlighted strains show 95% confidence interval of the mean. Examples shown are the GyrA hypomorph which is hypersensitive to the fluoroquinolone sarafloxacin (top left panel), the TrpG hypomorph which is hypersensitive to trimethoprim (bottom left), the RpoB hypomorph which is hypersensitive to RIF (top right), and the TrpA hypomorph which is hypersensitive to BRD-4592 (bottom right). (**D**) ROC curve of primary data against a confirmatory secondary growth assay. We retested more than 100 compounds using a resazurin-based colorimetric assay. Taking 50% inhibition in the secondary assay as ground truth, we demonstrated the primary assay as predictive of real activity that could be detected by more conventional growth methods.

thase inhibitor BRD-4592 (19) selectively inhibited the tryptophan synthase α-subunit (TrpA) hypomorph (Fig. 1C). Interestingly, TMP, a folate biosynthesis inhibitor, demonstrated a clear interaction with the hypomorph for the folate pathway enzyme glutamine amidotransferase (TrpG) rather than the DHFR hypomorph (Fig. S2A).

Across the screen, we tested for 1,290,400 possible chemical-genetic interactions, (3226 compounds × 100 strains × 4 concentrations) with the majority (927,025, 71%) being inhibitory (LFC < 0) (Fig. S2B). Of these, 55,508 interactions (6%), representing 940 compounds (29%), were strong (LFC < -2, $p < 10^{-10}$) and were considered hits. A minority of interactions indicated cases where protein depletion appeared to confer compound resistance, including identification of the known interaction between the mycothiol biosynthesis pathway enzyme cysteine ligase (MshC) hypomorph and the enoyl-[acyl-carrier-protein] reductase (InhA) inhibitors INH and ethionamide (ETH) (25).

We retested a sample of 112 specific hits (LFC < -2; $p < 10^{-10}$; specificity defined by activity against < 10 strains) for activity against wild type Mtb, each compound's strongest hypomorph interactor, and several other hypomorph strains that served as negative controls, using an orthogonal growth assay based on colorimetric resazurin detection. Because growth rates in different assays cannot be directly compared, we constructed a receiver operating characteristic (ROC) curve to determine how well inhibitory activity in the primary multiplex assay predicted activity in the secondary resazurin assay. Defining a confirmatory result in the secondary assay by a stringent cut-off of 50% growth inhibition compared to DMSO controls (Fig. 1D), the ROC area under the curve (AUC) was 0.73, indicating a high true positive rate in the primary assay with a well-controlled false positive rate. Given the complexity of the primary screen, we were reassured that 1375 (52%) of the 2664 extremely statistically significant interactions were confirmed in the secondary assay.

We recognize the potential value of the current primary data and chemical genetic interaction profiles identified in this study, exceeding those described here and the confines of our own laboratories and expertise, and thus are making data freely available as a resource to the community at https://broadinstitute.org/infectious-disease-microbiome/cgtb.

Identification of new inhibitors with specified MOAs by machine learning from known drugs

We next sought to use the resulting chemical-genetic interaction profiles to identify novel compounds with known MOAs. We applied supervised machine learning, leveraging the fact that 107 compounds in the compound library had known antimicrobial MOA (Table S4).

We visualized the 400-dimensional interaction profiles (Fig. 2A) for each compound through reduction to two dimensions using a t-distributed stochastic neighbor embedding (t-SNE) (26). Compounds known to have the same target clustered together, independent of their chemical structural similarities. This is illustrated with the protein synthesis inhibitors tylosin, erythromycin, and clindamycin (Fig. 2B).

The 107 compounds with known antimicrobial MOA included inhibitors of DNA gyrase ($n = 14$), mycolic acid synthesis ($n = 6$), and folate biosynthesis ($n = 12$). We trained separate binary classifiers using Lasso regression (27) to determine the chemical-genetic interaction profiles associated with each class, using 60% of the data as a training set and 40% as a test set.

DNA gyrase inhibitors. The 14 known DNA gyrase inhibitors in the compound collections were all fluoroquinolones. The regularized regression coefficients in the model suggested that the single most discriminatory feature was strongly decreased fitness of the GyrA hypomorph (Fig. S3A).

Among the compound library, the model predicted 55 non-quinolone DNA gyrase inhibitors (Fig. 3A), including novobiocin, a known inhibitor of the DNA gyrase β-subunit (GyrB). Both the GyrB and GyrA hypomorphs were hypersensitive to novobiocin, suggesting that the GyrA hypomorph could act as a sentinel strain for DNA gyrase inhibition in general.

To test these predictions, we obtained 52 of these compounds and assayed their ability to inhibit Mtb DNA gyrase supercoiling and decatenation activity *in vitro* (Fig. 3B and Fig. S3B). Of these, 27 (52%) showed significant activity. We also tested 25 randomly-chosen compounds predicted not to be DNA gyrase inhibitors; none showed activity. The classifier thus significantly enriched for DNA gyrase inhibitors ($p = 2 \times 10^{-7}$, Fisher's exact test; ROC AUC = 0.89).

Of the 55 non-quinolone compounds predicted to have DNA gyrase inhibitory activity, only one scaffold, ethacridine (Fig. 3C), has been previously reported to have activity against Mtb DNA gyrase (28). Interestingly, one of the predicted compounds, tryptanthrin, which has been the subject of extensive antibacterial and antitrypanosomal work (29, 30), previously had no understood MOA. We found that it inhibits *in vitro* decatenation at 160 μM and supercoiling at higher concentrations (Fig. S3B). This activity may account for its antimicrobial activity. Interestingly, the quinolone derivatives fleroxacin and nalidixic acid were predicted not to be DNA gyrase inhibitors in Mtb; this prediction was borne out *in vitro*.

Mycolic acid biosynthesis inhibitors. We next trained a model to predict new mycolic acid (MA) biosynthesis inhibitors by using the clinical antitubercular prodrugs INH and ETH, whose active forms both competitively inhibit InhA (31), a key enzyme in MA biosynthesis. Even though the strains tested did not include an InhA hypomorph, our analysis still yielded an excellent predictive model. The most discriminatory feature was increased relative fitness of the MshC hypomorph (Fig. S3C). MshC catalyzes the incorporation of cysteine into mycothiol, an antioxidant unrelated to MA biosynthesis. Consistent with this result, mycothiol biosynthesis deficiency has been shown to confer resistance to INH and ETH, probably through suppression of cysteine-induced

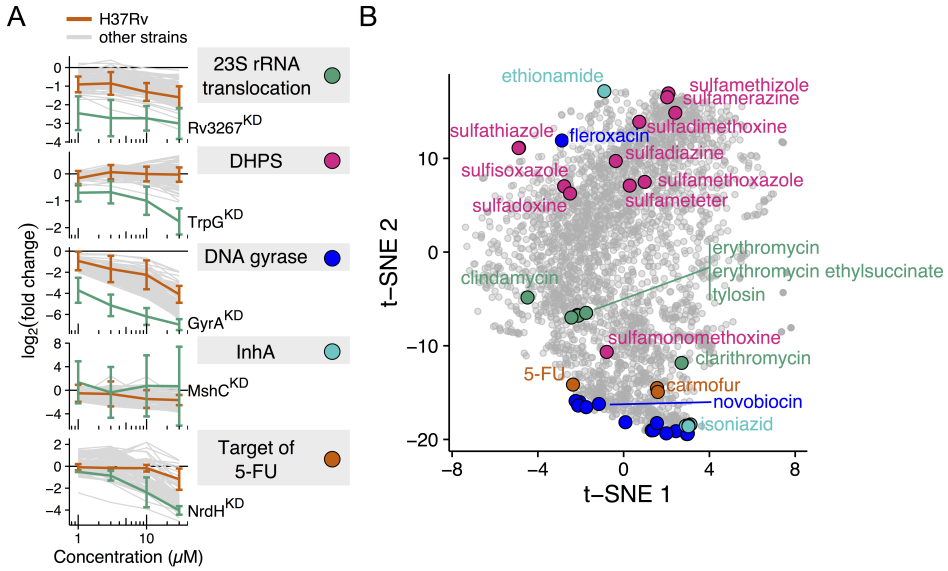

Figure 2: Unsupervised machine learning revealed an atlas of chemical genetic interactions in Mtb. (**A**) Centroid chemical genetic interaction profiles for compounds with the same MOAs, shown for inhibitors of 23S rRNA translocation inhibitors, dihydropteroate synthase (DHPS), DNA gyrase, InhA, and the several enzymes in the thymine biosynthesis pathway inhibited by 5-fluorouracil (5-FU). All strains are shown in grey, wild-type Mtb H37Rv in orange, and a relevant sentinel strain in green. Error bars show 95% confidence interval of the mean of the LFC (relative to DMSO negative controls) observed for all compounds known to have that particular MOA. (**B**) Using *t*-SNE to visualize the 400-dimensional dataset uncovered the MOA-driven clustering of compounds. For clarity, only five MOAs are illustrated here. Grey circles represent compounds, and colored circles represent a subset of compounds with known MOA: green for 23S rRNA translocation inhibitors, magenta for the sulfonamide dihydropteroate synthase (DHPS) inhibitors, dark blue for the DNA gyrase inhibitors, light blue for the InhA inhibitors, and orange for compounds related to 5-FU known to inhibit several enzymes in the thymine biosynthesis pathway.

respiration leading to reactive oxygen species (ROS)-mediated death (32).

Our model predicted seven compounds to be MA inhibitors (Fig. 3D), of which six were hydrazone derivatives of INH and one, BRD-9942, was an indenedione. All seven compounds inhibited wild-type Mtb growth at 50 μM or less in a broth microdilution assay, allowing us to test the effect of these compounds on wild-type Mtb. In a radiolabeling assay of MA biosynthesis, three INH hydrazones and BRD-9942 caused a detectable reduction in exogenous 14C-acetate incorporation into MA (Fig. 3E), validating that they act in the same pathway as INH. Further, a broth microdilution assay showed that an overexpressor of *inhA* (33) was resistant to the six INH-hydrazones, but not BRD-9942 (Fig. 3F, Fig. S3D).

The prodrug INH is activated by the catalase KatG, which cleaves its N–N bond (34). Because the INH hydrazones contain this bond, it seemed likely that they are activated in the same way. We confirmed this prediction by showing that the loss-of-function mutant Mtb *katGS315T* (*katG*$^-$) (35) was resistant to the INH hydrazones (Fig. S3D).

Folate biosynthesis inhibitors. We also built a predictor of folate biosynthesis inhibitors based on the chemical-genetic interaction profiles of the sulfonamides, which are known dihydropteroate synthase (DHPS) inhibitors; the most discriminatory feature was inhibition of the TrpG hypomorph (Fig. S4A). TrpG is involved in both folate and tryptophan (Trp) biosynthesis (Fig. S4B), catalyzing formation of both 4-amino-4-deoxychorismate (a folate precursor) and 2-amino-2-deoxyisochorismate (a Trp precursor).

The model predicted 43 compounds to be folate biosynthesis inhibitors (Fig. 3G), of which we tested seven, spanning several chemotypes. All showed inhibitory activity not only against the TrpG mutant but also wild-type Mtb at 200 μM or less. Hypothesizing that these compounds might be inhibitors of either folate or Trp biosynthesis, we tested whether their effects on wild-type Mtb were abolished by supplementation with Trp, folate, or the folate pathway intermediate *para*-amino benzoic acid (PABA). For reference, we also tested three known folate biosynthesis inhibitors with distinct activities: methotrexate (MTX, a DHFR inhibitor), *para*-amino salicylic acid (PAS, a prodrug that inhibits DHFR), and sulfanilamide (a dihydropteroate synthase (DHPS) inhibitor) (Fig. S4C). The two nitrothiophene compounds, BRD-2550 (Fig. S4D) and BRD-9819, behaved similarly in the supplementation assay (Fig. 3H) to MTX, with their effects abolished by both PABA and folate supplementation; this implied an analogous MOA to MTX. Notably, unlike any of the reference compounds, four predicted folate inhibitors including BRD-8884 (Fig. S4D) had effects that could only be rescued by folate (Fig. 3H), suggesting that they inhibit a novel, late step in the pathway. The effect of the final compound BRD-7721 (Fig. 3H), a 3-indolepropionic acid (3-IPA) ester (Fig. S4D), was only rescued by Trp supplementation, indicating that it is a Trp biosynthesis inhibitor. (3-IPA was recently identified as antimycobacterial (36); notably, 3-IPA's antitubercular effect is also abolished by Trp supplementation). By retraining on compounds whose effects were abolished by tryptophan versus folate or PABA supplementation, we found

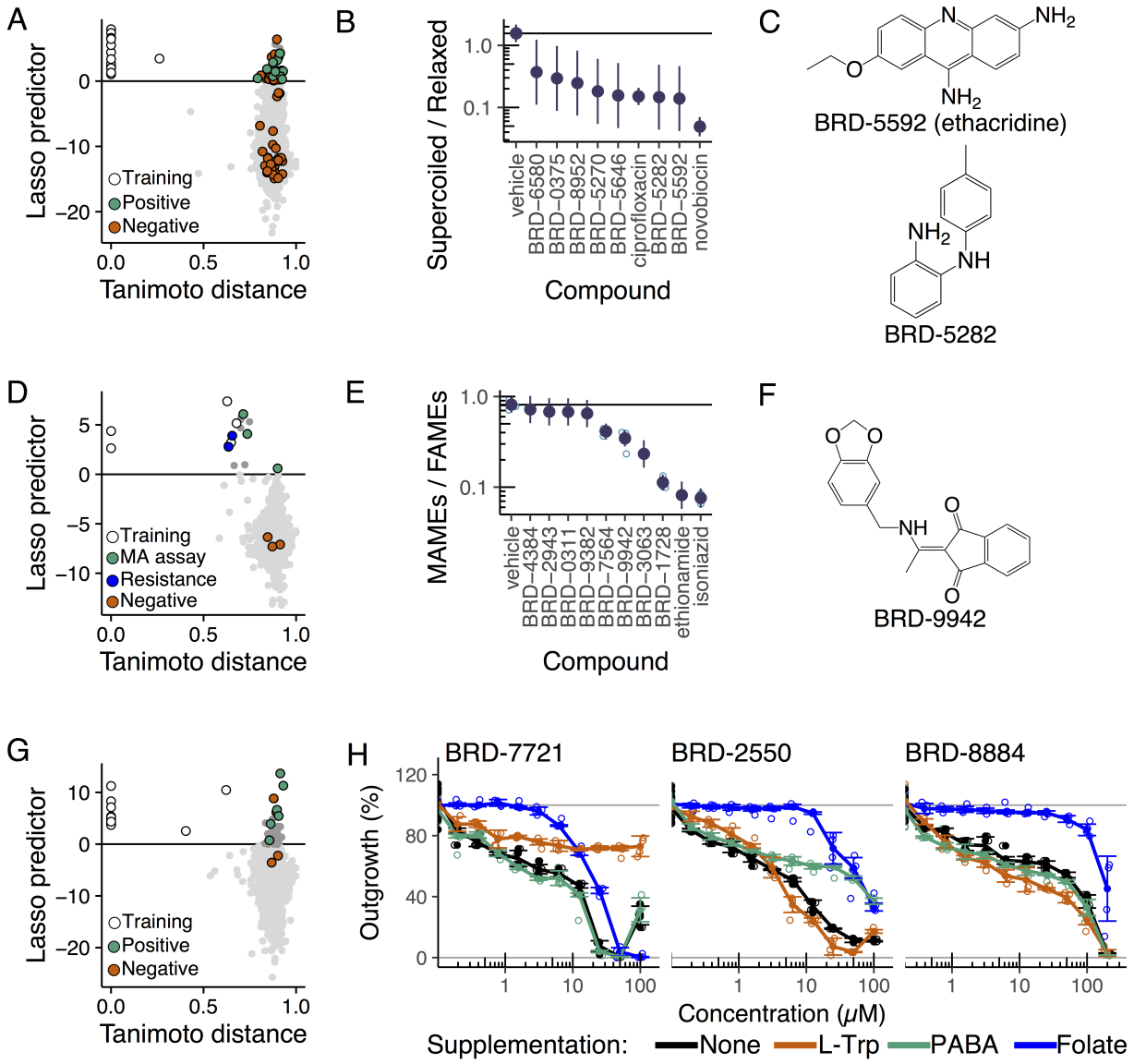

Figure 3: Supervised machine learning using Lasso binary classifiers uncovered new chemotypes for known MOAs. (**A**) Scatter plot of strength of prediction for DNA gyrase inhibition (Lasso predictor) against chemical structure dissimilarity to the fluoroquinolone family of known DNA gyrase inhibitors (Tanimoto distance). Each point is a compound in the screen. All compounds above the horizontal line were predicted to be DNA gyrase inhibitors. White points were known DNA gyrase inhibitors in the ground truth dataset. Compounds that were tested *in vitro* for DNA gyrase inhibition are shown in green (active) or orange (did not show activity). (**B**) Results of an *in vitro* assay of DNA gyrase supercoiling inhibition. DNA gyrase catalyzes supercoiling of relaxed plasmid DNA; when subjected to agarose gel electrophoresis, supercoiled plasmid runs faster than relaxed. The ratio of pixel intensities for supercoiled and relaxed bands was indicative of inhibition activity, as shown by the ciprofloxacin positive control. For clarity, only compounds which showed statistically significant ($p < 0.05$, Wald test) inhibition are shown. Error bars show standard errors of the GLM regression coefficients. (**C**) Examples of new DNA gyrase inhibitor chemotypes predicted by the Lasso classifier and confirmed *in vitro*. (**D**) As (A), but for the MA biosynthesis classifier. Green points indicate a positive *in vitro* result with the radiolabeled mycolic acid assay; blue points show compounds to which KatG– and BAA-812 were resistant. (**E**) Results of a radiolabeled 14C acetate incorporation assay for inhibition of mycolic acid biosynthesis. The ratio of pixel intensities for fatty acid methyl esters (FAMEs) and mycolic acid methyl esters (MAMEs) bands was indicative of inhibition activity, as shown by the isoniazid and ethionamide positive controls. Error bars show the 95% confidence interval of the GLM regression coefficients. (**F**) A new mycolic acid biosynthesis inhibitor chemotype predicted by the Lasso classifier and confirmed *in vitro*. (**G**) As (A), but for the folate classifier. (**H**) Representative dose response curves from the metabolite rescue assay of some compounds predicted, through TrpG hypomorph hypersensitivity, to be folate or tryptophan biosynthesis inhibitors. The effect of BRD-7721, a 3-indole propionic acid ester, is abolished by tryptophan supplementation, indicating it is a tryptophan biosynthesis inhibitor. In contrast, BRD-2550 (a nitrothiophene) and BRD-8884 are rescued by folate, showing that they are folate biosynthesis inhibitors. Individual replicates are shown as open circles, means are shown as filled circles, and error bars show 95% confidence intervals.

that the collateral strain depleted for dihydroneopterin aldolase (DHNA, encoded by *folB*), in conjunction with TrpG, could distinguish inhibitors of the two respective pathways (Fig. S4E–F). Altogether, this analysis identified novel inhibitors of folate biosynthesis, an important pathway that has been successfully exploited against many other pathogens, but to date, not Mtb.

Identification of new inhibitors against a specific target based on strain sensitivity

In the three examples above, we identified new compounds by training classifiers with data from known drugs with a specific MOA. We next sought to identify new compounds in situations where we lacked such information, by instead searching for compounds that selectively inhibited strains depleted for a specific target of interest.

We searched for inhibitors of the well-characterized and valuable target, RNAP, whose extremely potent clinical inhibitor RIF is credited with shortening TB chemotherapy. The RIF derivatives in our screen inhibited growth of all strains, providing no chemical-genetic signal for a machine learning model. However, we had tested RIF in the screen as a positive control across a wider concentration range and noted that the hypomorph of RpoB, a subunit of RNAP, was specifically inhibited at lower concentrations (Fig. 1C).

We identified 20 compounds that strongly inhibited ($p < 10^{-10}$, LFC < -2) the RpoB hypomorph, with it being among the two most inhibited strains for at least one dose (Fig. 4A). Recognizing that many mechanisms might lead to inhibition of an RNAP mutant, we tested the compounds to determine if any had activity in an *in vitro* RNA synthesis assay (37, 38). Importantly, three of the compounds (Fig. S5) showed direct inhibition of RNAP (Fig. 4B). Thus, compounds that specifically target the RpoB hypomorph are highly enriched for molecules that directly target RpoB itself. This example showed that new inhibitors can be identified based on activity against individual hypomorphic strains.

Screening a large chemical library

Our initial screen involved a library of 3226 compounds enriched for molecules with activity against wild-type Mtb. We next extended the approach to a large unbiased library of 47,353 compounds. This library was assembled from internal Broad Institute chemical libraries, including sub-libraries from the Broad diversity oriented synthesis collection (39), National Institutes of Health's Molecular Libraries Probe Production Centers Network library, and purchased from WuXi, filtered for physico-chemical properties including molecular weight < 550, calculated log(D) at pH 7.4 < 4, polar surface area < 110, charge at pH 7.4 > -1.

We screened these compounds (50 μM) against 152 strains (151 hypomorphs and wild-type), including 94 of the 100 strains used in the initial screen. Of the 7,245,009 potential chemical-genetic interactions tested, 95,685 (1.3%) scored as hits based on the criteria used in the initial screen. To validate the results, we repeated the assay using the 152-strain pool on 1331 compounds, which had specific activity against fewer than ten strains, and confirmed 78% of the chemical-genetic interactions previously identified as inhibitory (LFC < 0), resulting in an ROC AUC of 0.74.

We identified 436 compounds that were active against wild-type Mtb (0.9% hit rate); in contrast, 10-fold more compounds (4403; 9%) were active against at least one of the 152 strains. This 10% hit rate is ∼3-fold lower than the hit rate observed with the smaller, Mtb active enriched compound library (29%). Among the 3967 compounds that did not hit wild-type Mtb, 73% were highly specific (1-10 hypomorphic strains hit), 11% were moderately specific (11-50 strains hit) and the remaining 16% were relatively non-specific (more than 50 strains hit). This distribution shows greater specificity than for compounds in the small screen (35%, 31%, and 34%), likely due to the enrichment for compounds with wild-type Mtb activity in the smaller library (Fig. S6A). Notably, the pattern of strain sensitivity showed considerable diversity: 59% of the strains tested in the smaller screen were the strongest hit for at least one compound at 30 μM, and the proportion was 75% in the larger screen–suggesting that compounds can be found against much of the target space. For the 94 strains that were common to both screens, there was strong correlation between the number of hit compounds against each strain in the two screens (log-transformed Pearson's $r = 0.8$) (Fig. S6B).

The larger screen demonstrates that our chemical-genomic approach should be applicable to any chemical library. Moreover, it should identify many more chemical hits than screening wild-type Mtb alone and associate them with activity against specific hypomorphs.

Developing wild-type activity of a compound discovered through hypomorph screening

While our approach identifies ∼10-fold more compounds than screening against wild-type Mtb and sheds light about the compounds' targets, its utility for drug development depends on the ability to optimize hits against the hypomorphs to molecules with pharmacologically relevant activity against wild-type Mtb. We therefore sought to demonstrate that it was possible to perform such optimization.

To identify the attractive hits for optimization, we excluded compounds with activity against wild-type Mtb, ranked compound-strain interactions based on specificity (how few other strains were significantly inhibited by the compound), susceptibility of strains at each concentration, and whether the compound contained chemically promising scaffolds. The highest ranked compound was BRD-8000, which across all four concentrations specifically inhibited the growth of the hypomorph of EfpA (Fig. 4C), a largely uncharacterized, but essential efflux pump in Mtb. In a separate broth microdilution assay, we confirmed that BRD-8000 showed strong activity against the EfpA hypomorph ($MIC_{90} = 6$ μM). By contrast, the compound showed no wild-type activity in the

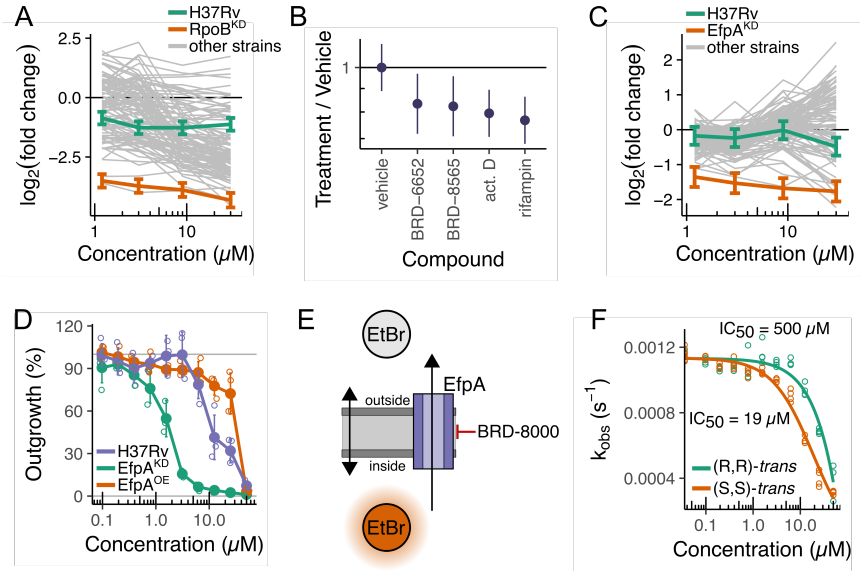

Figure 4: Identification of inhibitors of known and previously uncharacterized targets by their unique interaction with a specific hypomorph. (**A**) Chemical genetic interaction profile of the antineoplastic RNAP inhibitor actinomycin D. The RpoB hypomorph was consistently hypersensitive across the four concentrations of the screen. (**B**) Results of an *in vitro* assay for inhibition of RNA synthesis by E. coli RNAP. Four compounds out of 20 selected for RpoB hypomorph specificity were confirmed as E. coli RNAP inhibitors. Only compounds which showed statistically significant ($p < 0.05$, Wald test) inhibition are shown. Error bars show the 95% confidence interval of the GLM regression coefficients. Act. D: actinomycin D. (**C**) Chemical genetic interaction profile of new, putative EfpA-inhibitor BRD-8000. The essential efflux pump EfpA hypomorph was consistently hypersensitive across the four concentrations of the screen. (**D**) EfpA-targeting by BRD-8000 was orthogonally corroborated by broth microdilution assay, showing hypersensitivity of the EfpA hypomorph to BRD-8000 compared to wild-type Mtb H37Rv, and moderate resistance of an EfpA overexpressor strain to BRD-8000. (**E**) Cartoon representing the principle of the EtBr efflux assay. EtBr is assumed to diffuse passively into the bacterial cell, where it becomes much more fluorescent. An observed efflux rate can be determined by measuring the time-dependent decay in fluorescence. (**F**) An EtBr efflux assay showed a large difference in efflux inhibition between the active (S,S)-*trans* ($IC_{50} = 19$ μM) and the inactive (R,R)-*trans* ($IC_{50} = 500$ μM) enantiomers of BRD-8000.2. The observed first-order rate constant for efflux decreases in a dose-dependent manner with BRD-8000 series compounds. Further investigation of the mechanism is shown in Fig. S7B–E.

screen and only weak activity in the broth microdilution assay ($MIC_{90} \geq 50$ μM) (Fig. 4D).

To optimize BRD-8000, we began by focusing on the fact that it is a mixture of stereoisomers. We found that the (S,S)-*trans* stereoisomer was the active form (BRD-8000.1; Table 1), with a wild-type $MIC_{90} = 12.5$ μM, which is greater than four-fold lower than that of the corresponding BRD-8000 mixture. We further increased the potency by moving the pyridyl bromine from the 5- to the 6-position to obtain BRD-8000.2 ($MIC_{90} = 3$ μM). The initial and optimized compounds showed similar differential activity (30-fold) with respect to inhibition of the EfpA hypomorph (Table 1), suggesting that the optimized compound remained on-target.

With the increased potency of BRD-8000.2, we obtained genetic evidence for EfpA as the target by generating resistant mutants in wild-type Mtb H37Rv. We obtained more than 30 independent resistant clones ($MIC_{90} > 50$ μM, Fig. S7A), each with a C955A mutation in *efpA* (coding for $EfpA_{V319F}$), occurring at a resistance frequency of $\sim 10^{-8}$.

We sought to functionally confirm that the BRD-8000 series targets EfpA by taking advantage of the fact that it does not inhibit growth of *Mycobacterium smegmatis* (Msm), likely because EfpA is not essential in Msm (40). We assayed the compound's effect on EfpA efflux activity in Msm by loading cells with the dye ethidium bromide (EtBr), a substrate of the pump, and then measuring efflux, since EtBr fluorescence is 20-fold higher when the dye is intracellular than extracellular (41). We determined that both BRD-8000 and BRD-8000.2 directly inhibited efflux in living cells, with an IC_{50} of 37 μM and 15 μM, respectively (Fig. S7B). This inhibition was stereospecific as the inactive (R,R)-*trans* isomer of BRD-8000.2 has an efflux IC_{50} of 500 μM (Fig. 4F). BRD-8000.2 is not a competitive substrate for EfpA, as its inhibition has an inverse relationship with initial EtBr concentration, suggesting an uncompetitive or non-competitive inhibitory mechanism (Fig. S7C, Fig. S7D). We also found that the IC_{50} for the compound was substantially higher in an *efpA* knockout strain of Msm than in wild-type Msm (Fig. S7E), indicating that BRD8000.2 has an EfpA-specific higher-potency interaction; episomal complementation of the knockout with the Mtb *efpA* gene restored the lower IC_{50} (Fig. S7F).

We found that BRD-8000.2 is bactericidal (Fig. S7G), has low human toxicity (hepatocyte $IC_{50} = 100$ μM), and does not act on bacteria lacking an essential EfpA homolog, including conventional species such as *Staphylococcus aureus*, *Pseudomonas aeruginosa*, and *Klebsiella pneumoniae*. These properties, including the narrow spectrum of activity, are favorable for therapeutic potential for BRD-8000.2 against Mtb.

More broadly, the results for BRD-8000.2 and EfpA demonstrate the potential of chemical screening of hypomorph libraries to yield promising small molecule candidates with wild-type activity that would otherwise elude discovery and development.

Compound	Structure	MIC_{90} (μM) H37Rv	MIC_{90} (μM) $EfpA^{KD}$
BRD-8000	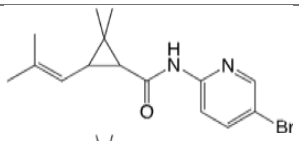	50	6.0
BRD-8000.1	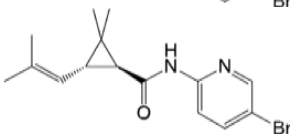	12.5	0.6
BRD-8000.11	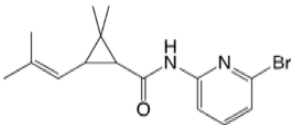	12.5	0.6
BRD-8000.2	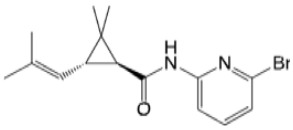	3.0	0.2

Table 1: Potencies of compounds targeting the essential efflux pump EfpA. MIC_{90}: Minimum inhibitory concentration at 90%; $EfpA^{KD}$: EfpA hypomorph.

Discussion

We developed a powerful and rapid systems chemical biology strategy both to discover many potential compounds for drug development against Mtb and to gain insights about their MOA. Using a pool of barcoded Mtb strains that are each depleted for a different essential gene product, we performed multiplexed screens with small-molecule libraries and used high-throughput barcode sequencing to estimate the census of each strain following chemical perturbations. Based on predictions from the chemical-genetic profiles of primary screening data, we readily identified MOA for 45 molecules. Importantly, these hits included new scaffolds against both known and new targets. With chemical optimization, we generated a new inhibitor of a new target, EfpA, active in wild-type Mtb. We also demonstrated that screening of genetic libraries identified ∼10-fold more hits than obtained by screening wild-type Mtb alone.

Chemical-genetic screens were first reported in yeast, taking advantage of the ability to deplete essential targets through heterozygosity for gene knockouts (42). This approach is not possible in bacteria, because they are haploid. Instead, chemical-genetic screens have been performed in *E. coli* using strains carrying deletions of non-essential genes (7, 43-45). But, this approach is limited to non-essential genes, which are generally not drug targets. In yeast and *E. coli*, it is sometimes possible to make inferences about the MOA of drugs against the products of essential genes based on the sensitivity of strains deleted for non-essential genes, by using extensive prior knowledge of genetic interaction networks in these exhaustively studied model organisms. By contrast, Mtb lacks these advantages: 45% of gene functions cannot be assigned by homology, and 27% of its genes are totally uncharacterized (46, 47).

In principle, libraries of hypomorphic strains with varying levels of knockdown provide a way to studying chemical-genetic interactions involving essential genes. In 2009, Donald *et al.* characterized 58 known *Staphylococcus aureus* inhibitors by screening them against 101 strains with significant knockdowns of essential genes (48). However, this approach has not been widely used.

Here, we show that a genetic knock-down library of essential genes can be constructed in Mtb, can be used for chemical screening, and can shed light on MOA even without well-understood networks (8). We used the resulting chemical genetic interaction profiles to predict new inhibitors of known targets, finding and validating 41 new chemical scaffolds that target new DNA gyrase, MA biosynthesis, and folate biosynthesis, based on the similarity of their profiles with those of drugs against these known targets. We found that some MOAs were predicted by the behavior of predominantly one strain – defined as the pathway sentinel strains– such as the GyrA hypomorph for DNA gyrase. It may be possible, therefore, to define a minimal subset of pathway sentinels that allow prediction of any MOA. (Such an approach is used to infer the transcriptional response of cancer cells to drug treatment, based on the response of ∼1000 genes, out of the ∼20,000 in the human genome (49)). In some cases however, collateral information from multiple strains aided MOA assignment, as illustrated by the refinement of TrpG-based folate and tryptophan biosynthesis inhibitor prediction using collateral strain behavior (the DHNA hypomorph). Additionally, collateral mutants allowed MOA prediction in the absence of the hypomorph corresponding to the actual target or of a sentinel strain, as illustrated by the ability to identify MA biosynthesis inhibitors in the absence of an InhA hypomorph. Determining the optimal balance of strains to screen will require increased understanding of pathway sentinels, core vulnerabilities, and Mtb's genetic interaction networks, all of which will facilitate iterative improvement of MOA prediction.

In a complementary approach that underscores the power of our systems chemical biology strategy, we also predicted MOA of targets without relying on the genetic interaction profiles of known drugs. By prioritizing of compounds based on the identity of and selectivity for particular hypersensitive mutants, we found three new inhibitors of RNAP; RNAP is the high value target of the first-line drug RIF and new inhibitors have been elusive. Excitingly, we also found an inhibitor of an entirely novel target in our discovery of the EfpA-inhibitor BRD-8000. While the initial hit had little wild-type Mtb activity, subsequent optimization yielded a molecule, BRD-8000.2, with clinically relevant potency against wild-type Mtb, on par with current antitubercular drugs. These results illustrate the value of the primary screening data for early elucidation of MOA, the ability to access novel small-molecule candidates that would elude traditional methods of screening wild-type Mtb, and the ability to identify inhibitors of novel targets even in the absence of well-characterized target function.

The ability to leverage the much greater hit rate from screening pooled hypomorphs and to chemically optimize hits to obtain wild-type activity has the potential to revolutionize the process of Mtb drug discovery, by making it possible to identify and prioritize both targets and compounds based on chemical-genetic interaction profiles. We are hopeful that the approach will substantially expand the number and target diversity of drug leads for development and eventual human clinical testing. The next steps involve completing the genetic libraries to encompass all essential genes; large-scale screening of diverse chemical libraries; development of new analytical methods to infer MOA; and further efforts to optimize hits against hypomorphs to clinically relevant drug leads.

References

1. "Global tuberculosis report 2017," (World Health Organization, Geneva, 2017).
2. E. W. Emmart, The tuberculostatic action of streptothricin and streptomycin with special reference to the action of streptomycin on the chorioallantoic membrane of the chick embryo. *Public Health Rep.* 60, 1415-1421 (1945).
3. K. Dheda et al., The epidemiology, pathogenesis, transmission, diagnosis, and management of multidrug-resistant, extensively drug-resistant, and incurable tuberculosis. *The Lancet Respiratory Medicine* 5, 291-360 (2017).
4. T. Christophe et al., High content screening identifies decaprenyl-phosphoribose 2' epimerase as a target for intracellular antimycobacterial inhibitors. PLoS Pathog. 5, e1000645 (2009).
5. A. E. Grzegorzewicz et al., Inhibition of mycolic acid transport across the *Mycobacterium tuberculosis* plasma membrane. *Nat. Chem. Biol.* 8, 334-341 (2012).
6. S. A. Stanley et al., Diarylcoumarins inhibit mycolic acid biosynthesis and kill *Mycobacterium tuberculosis* by targeting FadD32. *Proc. Natl. Acad. Sci. U. S. A.* 110, 11565-11570 (2013).
7. A. Typas et al., High-throughput, quantitative analyses of genetic interactions in *E. coli*. *Nat. Methods* 5, 781-787 (2008).
8. J. Wang et al., Platensimycin is a selective FabF inhibitor with potent antibiotic properties. *Nature* 441, 358-361 (2006).
9. J. C. Evans et al., Validation of CoaBC as a Bactericidal Target in the Coenzyme A Pathway of *Mycobacterium tuberculosis*. *ACS Infectious Disease* 2, 958-968 (2016).
10. G. L. Abrahams et al., Pathway-selective sensitization of *Mycobacterium tuberculosis* for target-based whole-cell screening. *Chem. Biol.* 19, 844-854 (2012).
11. M. A. DeJesus et al., Comprehensive Essentiality Analysis of the *Mycobacterium tuberculosis* Genome *via* Saturating Transposon Mutagenesis. *MBio* 8, (2017).
12. J. H. Kim et al., Protein inactivation in mycobacteria by controlled proteolysis and its application to deplete the beta subunit of RNA polymerase. *Nucleic Acids Res.* 39, 2210-2220 (2011).
13. J. H. Kim et al., A genetic strategy to identify targets for the development of drugs that prevent bacterial persistence. *Proc. Natl. Acad. Sci. U. S. A.* 110, 19095-19100 (2013).
14. C. Yu et al., High-throughput identification of genotype-specific cancer vulnerabilities in mixtures of barcoded tumor cell lines. *Nat. Biotechnol.* 34, 419-423 (2016).
15. T. X. Han, X.-Y. Xu, M.-J. Zhang, X. Peng, L.-L. Du, Global fitness profiling of fission yeast deletion strains by barcode sequencing. *Genome Biol.* 11, R60-R60 (2010).
16. A. M. Smith et al., Highly-multiplexed barcode sequencing: An efficient method for parallel analysis of pooled samples. *Nucleic Acids Res.* 38, 1-7 (2010).
17. A. M. Smith et al., Quantitative phenotyping *via* deep barcode sequencing. *Genome Res.* 19, 1836-1842 (2009).
18. S. S. Grant et al., Identification of novel inhibitors of nonreplicating *Mycobacterium tuberculosis* using a carbon starvation model. *ACS Chem. Biol.* 8, 2224-2234 (2013).
19. S. Wellington et al., A small-molecule allosteric inhibitor of *Mycobacterium tuberculosis* tryptophan synthase. *Nat. Chem. Biol.* 13, 943-950 (2017).
20. S. A. Stanley et al., Identification of novel inhibitors of *M. tuberculosis* growth using whole cell based high-throughput screening. *ACS Chem. Biol.* 7, 1377-1384 (2012).
21. R. C. Reynolds et al., High throughput screening of a library based on kinase inhibitor scaffolds against *Mycobacterium tuberculosis* H37Rv. *Tuberculosis (Edinb)* 92, 72-83 (2012).
22. S. Ananthan et al., High-throughput screening for inhibitors of *Mycobacterium tuberculosis* H37Rv. *Tuberculosis (Edinb)* 89, 334-353 (2009).
23. J. A. Maddry et al., Antituberculosis activity of the molecular libraries screening center network library. *Tuberculosis (Edinb)* 89, 354-363 (2009).
24. L. Ballell et al., Fueling open-source drug discovery: 177 small-molecule leads against tuberculosis. *ChemMedChem* 8, 313-321 (2013).
25. C. Vilchèze et al., Coresistance to isoniazid and ethionamide maps to mycothiol biosynthetic genes in Mycobacterium bovis. *Antimicrob. Agents Chemother.* 55, 4422-4423 (2011).
26. L. van der Maaten, Accelerating *t*-SNE using Tree-Based Algorithms. *Journal of Machine Learning Research* 15, 3221-3245 (2014).
27. R. Tibshirani, Regression Shrinkage and Selection *via* the Lasso. *J. Roy. Stat. Soc. Ser. B. (Stat. Method.)* 58, 267 (1994).
28. B. Medapi, N. Meda, P. Kulkarni, P. Yogeeswari, D. Sriram, Development of acridine derivatives as selective *Mycobacterium tuberculosis* DNA gyrase inhibitors. *Bioorg. Med. Chem.* 24, 877-885 (2016).
29. J. Scovill, E. Blank, M. Konnick, E. Nenortas, T. Shapiro, Antitrypanosomal Activities of Tryptanthrins. *Antimicrob. Agents Chemother.* 46, 882-883 (2002).
30. J. M. Hwang et al., Design, synthesis, and structure-activity relationship studies of tryptanthrins as antitubercular agents. *J. Nat. Prod.* 76, 354-367 (2013).
31. A. Banerjee et al., InhA, a Gene Encoding a Target for Isoniazid and Ethionamide in *Mycobacterium tuberculosis*. *Science* 263, 227-330 (1994).

32. C. Vilchèze et al., Enhanced respiration prevents drug tolerance and drug resistance in *Mycobacterium tuberculosis*. *Proc. Natl. Acad. Sci. U. S. A.* 114, 4495-4500 (2017).

33. B. M. Madison et al., Identification of a *Mycobacterium tuberculosis* Strain with Stable, Low-Level Resistance to Isoniazid. *J. Clin. Microbiol.* 42, 1294-1295 (2004).

34. Y. Zhang, B. Heym, B. Allen, D. Young, S. Cole, The catalase-peroxidase gene and isoniazid resistance of *Mycobacterium tuberculosis*. *Nature* 358, (1992).

35. S. Yu, S. Girotto, C. Lee, R. S. Magliozzo, Reduced affinity for Isoniazid in the S315T mutant of *Mycobacterium tuberculosis* KatG is a key factor in antibiotic resistance. *J. Biol. Chem.* 278, 14769-14775 (2003).

36. D. A. Negatu et al., Whole-Cell Screen of Fragment Library Identifies Gut Microbiota Metabolite Indole Propionic Acid as Antitubercular. *Antimicrob. Agents Chemother.* 62, (2018).

37. E. T. Kool. (University of Rochester, United States, 2000).

38. S. L. Daubendiek, E. T. Kool, Generation of catalytic RNA by rolling transcription of synthetic DNA nanocircles. *Nat. Biotechnol.* 15, 273-277 (1997).

39. D. H. Chou et al., Synthesis of a novel suppressor of beta-cell apoptosis *via* diversity-oriented synthesis. *ACS Med. Chem. Lett.* 2, 698-702 (2011).

40. X. Z. Li, L. Zhang, H. Nikaido, Efflux pump-mediated intrinsic drug resistance in *Mycobacterium smegmatis*. *Antimicrob. Agents Chemother.* 48, 2415-2423 (2004).

41. L. Paixao et al., Fluorometric determination of ethidium bromide efflux kinetics in *Escherichia coli*. *J. Biol. Eng.* 3, 18 (2009).

42. G. Giaever et al., Genomic profiling of drug sensitivities *via* induced haploinsufficiency. *Nat. Genet.* 21, 278-283 (1999).

43. J. Wildenhain et al., Prediction of Synergism from Chemical-Genetic Interactions by Machine Learning. *Cell Syst* 1, 383-395 (2015).

44. L. Pasquina et al., A synthetic lethal approach for compound and target identification in *Staphylococcus aureus*. *Nat. Chem. Biol.* 12, 40-45 (2016).

45. J. S. Piotrowski et al., Functional annotation of chemical libraries across diverse biological processes. *Nat. Chem. Biol.* 13 982-993 (2017).

46. M. M. Jaafar et al., Genome Sequencing and Annotation of *Mycobacterium tuberculosis* PR08 strain. *Genom Data* 7, 119-120 (2016).

47. T. Doerks, V. van Noort, P. Minguez, P. Bork, Annotation of the *M. tuberculosis* hypothetical orfeome: adding functional information to more than half of the uncharacterized proteins. *PLoS One* 7, e34302 (2012).

48. R. G. Donald et al., A *Staphylococcus aureus* fitness test platform for mechanism-based profiling of antibacterial compounds. *Chem. Biol.* 16, 826-836 (2009).

49. A. Subramanian et al., A Next Generation Connectivity Map: L1000 Platform and the First 1,000,000 Profiles. *Cell* 171, 1437-1452 e1417 (2017).

50. M. I. Love, W. Huber, S. Anders, Moderated estimation of fold change and dispersion for RNA-seq data with DESeq2. *Genome Biol.* 15, 550 (2014).

Acknowledgements

The raw primary screen data and calculated log fold changes and p-values are available online at https://broadinstitute.org/infectious-disease-microbiome/cgtb. Funding was provided by Bill and Melinda Gates Foundation, Broad Institute TB Gift Donors and Pershing Square Foundation.